Electronic Supplementary Material (ESI) for Physical Chemistry Chemical Physics.
This journal is © the Owner Societies 2021

# Supporting information

## Prediction of Bimetal Embedded in Two-Dimensional Materials for $CO_2$ Reduction Electrocatalysis with a New Integrated Descriptor

*Xin Cao,*[‡] *Chongyang Chen,*[‡] *Yuxiang Min,*[‡] *Hao Yuan,*[‡] *Shiqian Chen,*[‡] *and Lai Xu*[*]

Institute of Functional Nano & Soft Materials (FUNSOM), Jiangsu Key Laboratory for Carbon-based Functional Materials & Devices, Soochow University, Suzhou, Jiangsu 215123, China

Email: xulai15@suda.edu.cn

**Table S1.** Gibbs free energy changes for the step of $*CO_2 \rightarrow *COOH$ or $H*COO$, compared with HER.

| System | $\Delta G_{*COOH}$ (eV) | $\Delta G_{*HCOO}$ (eV) | $\Delta G_{*HER}$ (eV) |
|---|---|---|---|
| ScSc | 0.794 | -0.935 | -0.264 |
| MnMn | -0.109 | -0.604 | 0.139 |
| FeFe | -0.122 | -0.572 | 0.008 |
| VV | -0.256 | -1.620 | 0.753 |
| TiTi | 0.107 | -1.127 | -0.030 |
| TiNi | 0.834 | -0.847 | -0.396 |
| VNi | 0.732 | -0.885 | -0.193 |
| ScNi | -0.102 | -0.274 | 0.239 |
| MnNi | 0.329 | -0.220 | -0.100 |
| FeNi | 0.144 | -1.046 | -0.016 |
| ScCu | 0.485 | -0.928 | 0.087 |
| TiCu | 0.505 | -0.972 | 0.547 |
| FeCu | -0.308 | -0.793 | 0.777 |
| ScCo | 1.141 | -0.508 | 0.148 |
| TiCo | 0.852 | -0.652 | 0.185 |
| MnCo | 0.205 | -0.510 | 0.470 |
| FeCo | -0.254 | -0.068 | 0.490 |
| ScFe | 2.805 | -0.327 | -0.101 |
| TiFe | 0.805 | -0.625 | -0.014 |
| VFe | -0.026 | -1.381 | -0.143 |
| CrFe | -0.013 | -1.079 | -0.126 |
| MnFe | 0.084 | -0.805 | 0.277 |
| ScMn | 0.426 | -0.810 | -0.152 |
| TiMn | 0.260 | -1.266 | -0.029 |
| VMn | 0.158 | -1.198 | 0.011 |
| CrMn | -0.135 | -1.275 | 0.115 |
| ScCr | -0.486 | -1.518 | 0.040 |
| TiCr | -0.030 | -1.539 | 0.137 |
| ScV | -0.363 | -1.408 | 0.195 |
| TiV | -0.060 | -1.407 | -0.520 |
| ScTi | -0.390 | -1.155 | 0.198 |

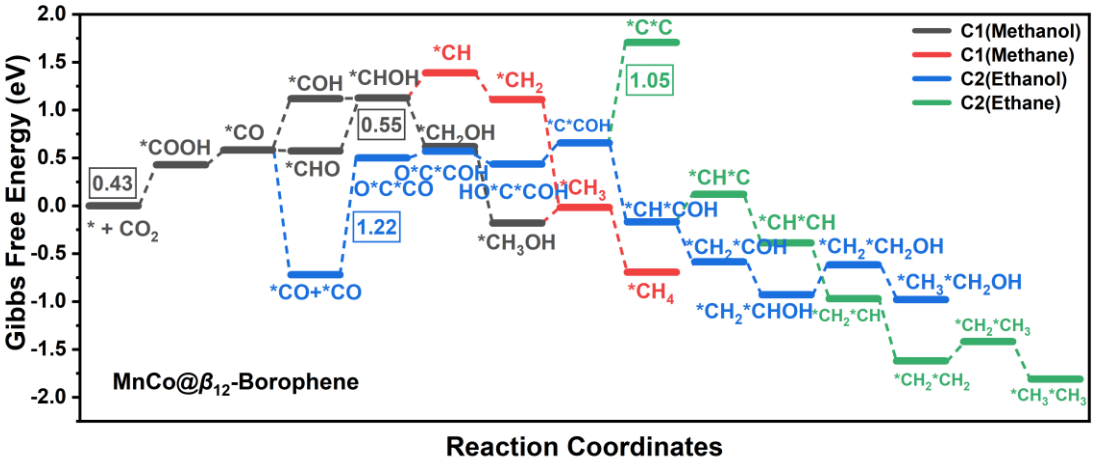


**Figure S1.** Gibbs free energy changes for reduction of $CO_2$ to methanol (black), methane(red), ethane(green)and ethanol(sky-blue) for MnCo@$\beta_{12}$-B system.

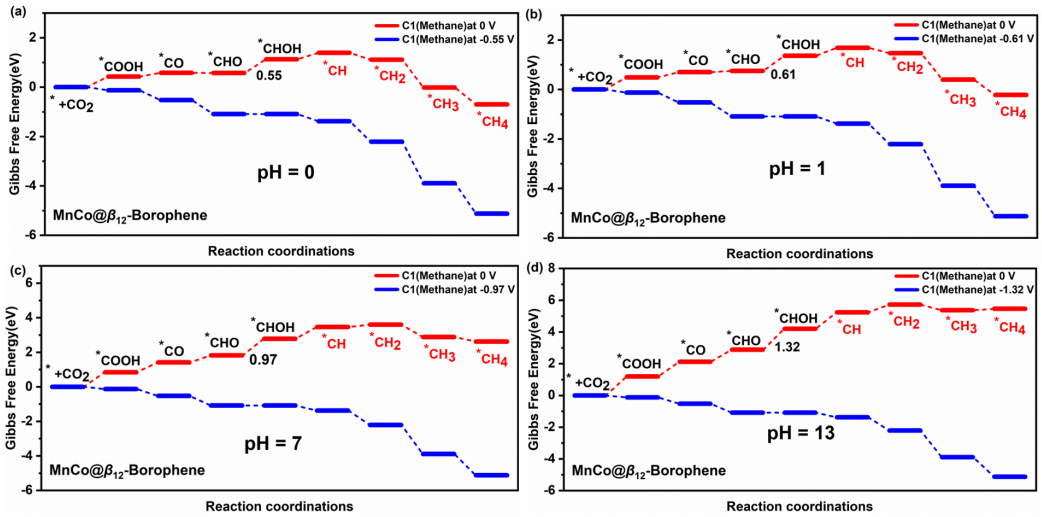


**Figure S2.** Gibbs free energy changes for reduction of $CO_2$ to methane(red), for MnCo@$\beta_{12}$-B system at pH=0(a), pH=1(b), pH=7(c), pH=13(d). The blue line represents the Gibbs free energy change under different applied voltages.

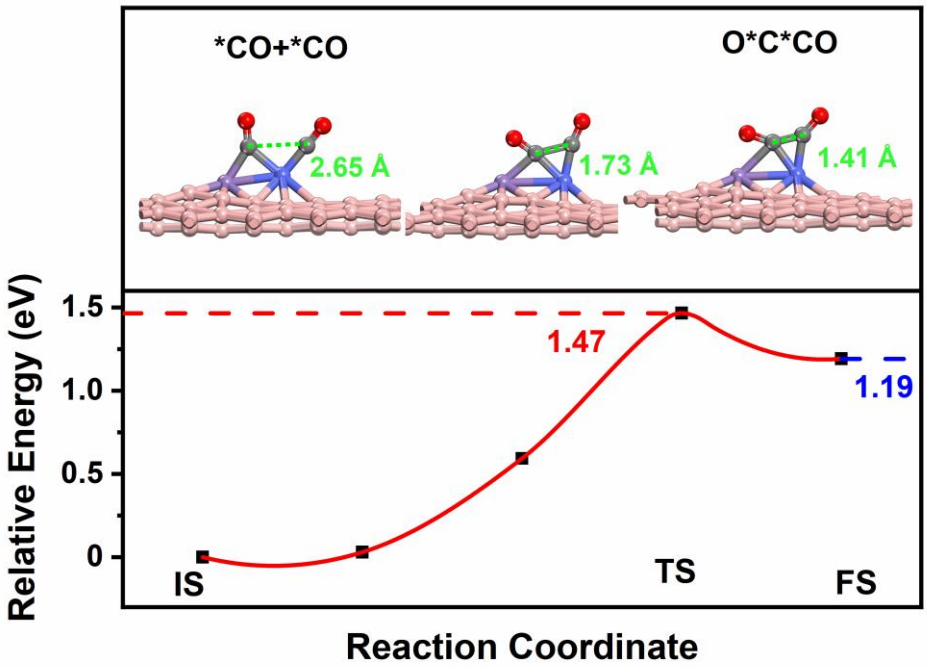


**Figure S3.** The side view of IS, TS, and FS structure and energy barrier diagram involved in the reaction *CO + *CO → O*C*CO for MnCo@$\beta_{12}$-B system.

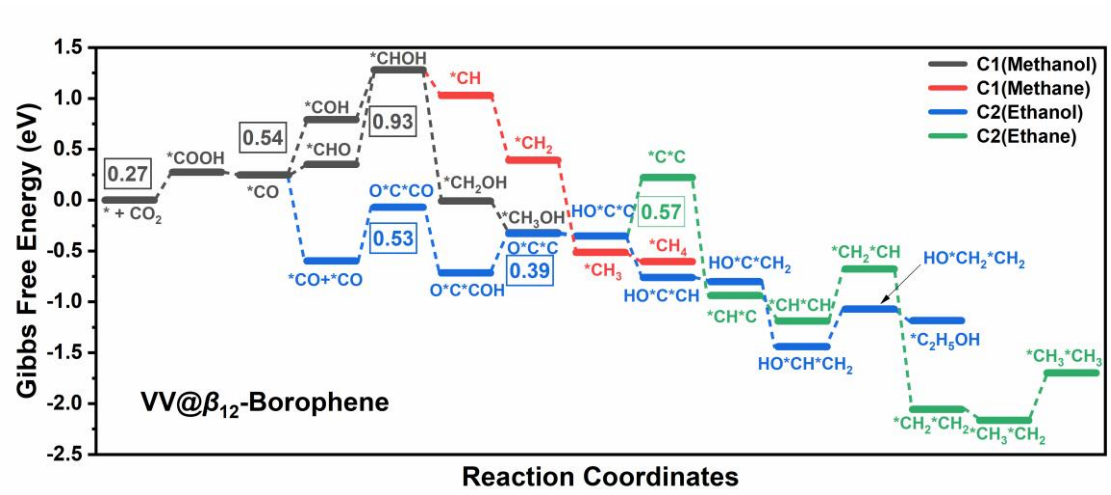


**Figure S4.** Gibbs free energy changes for reduction of $CO_2$ to methanol (black), methane(red), ethane(green) and ethanol(sky-blue) for VV@$\beta_{12}$-B system.

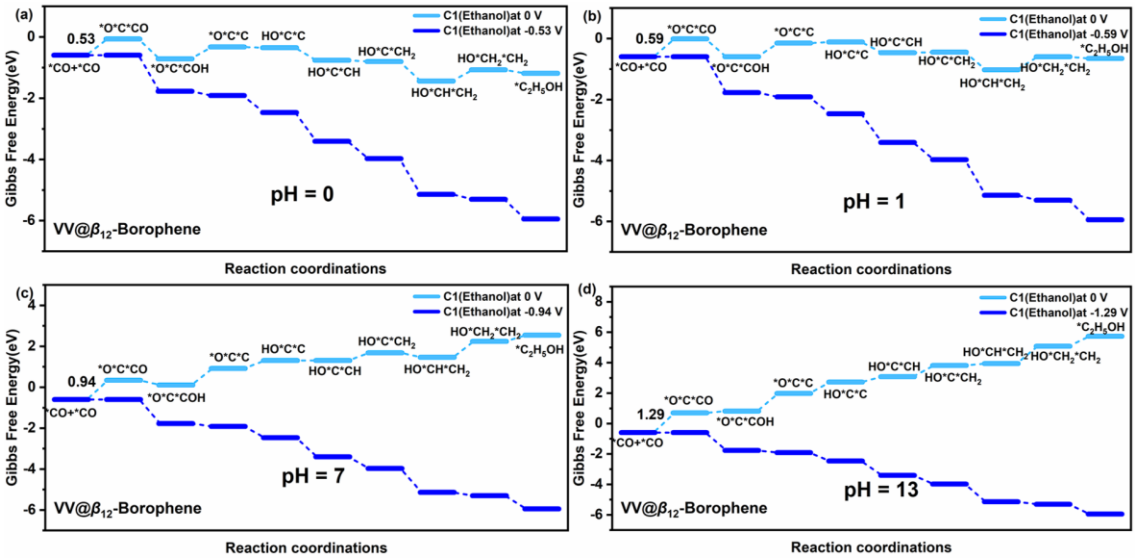


**Figure S5.** Gibbs free energy changes for reduction of $CO_2$ to ethanol(sky-blue), for VV@$\beta_{12}$-B system at pH=0(a), pH=1(b), pH=7(c), pH=13(d). The blue line represents the Gibbs free energy change under different applied voltages.

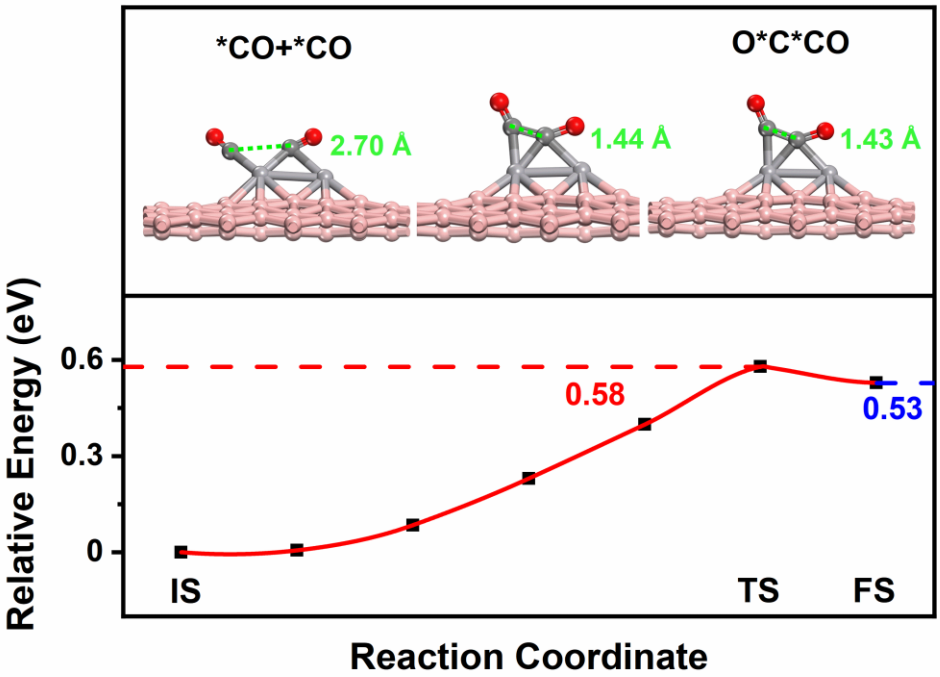


**Figure S6.** The side view of IS, TS, and FS structure and energy barrier diagram involved in the reaction *CO + *CO → O*C*CO for VV@$\beta_{12}$-B system.

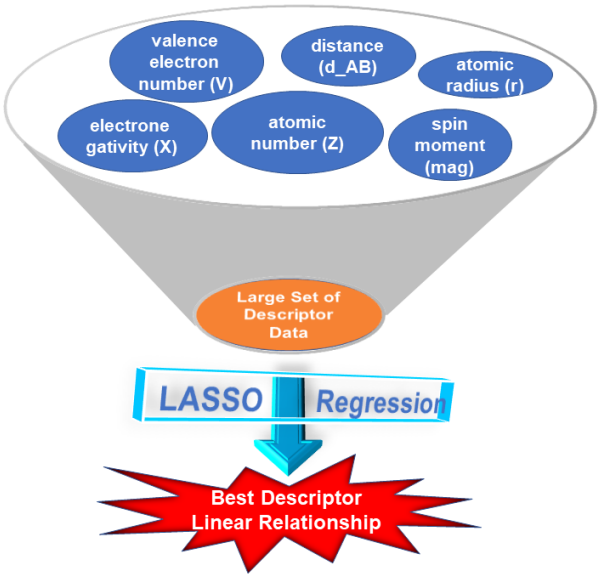


**Figure S7**. Schematic diagram of LASSO regression looking for descriptors.

**Table S2.** The distance between two transition metals and the spin moments of the transition metals A and B in the magnetic system.

| A | B | spin moment (A, μB) | spin moment (B, μB) | Distance (Å) |
|---|---|---|---|---|
| Fe | Fe | 1.11 | 1.07 | 2.56 |
| Ni | Mn | -0.04 | 1.74 | 2.57 |
| Mn | Co | 1.85 | 0.07 | 2.59 |
| Fe | Co | 1.40 | -0.05 | 2.55 |
| Ti | Fe | 0.21 | 1.63 | 3.08 |
| Cr | Fe | 1.04 | 1.51 | 2.77 |
| Mn | Fe | 1.32 | 1.74 | 2.62 |
| Ti | Mn | 0.24 | 2.14 | 2.96 |
| V | Mn | 0.26 | 2.03 | 2.78 |
| Cr | Mn | 1.36 | 2.09 | 2.77 |

**Table S3.** Possible pathways for electrochemical reduction of $CO_2$. Limiting potentials(V) and overpotentials(V) of MnCo and VV system respectively. $U_0$ was obtained from the source.[1]

| Half-electrochemical thermodynamic reaction | $U_0$/(V) | $U_L$/(V) | $\eta$/(V) |
|---|---|---|---|
| MnCo : $CO_2(g) + 8H^+ + 8e^- = CH_4(g) + 2H_2O(l)$ | 0.16 | -0.55 | 0.71 |
| MnCo : $2CO_2(l) + 12H^+ + 12e^- = CH_3CH_2OH(l) + 3H_2O(l)$ | 0.08 | -1.22 | 1.30 |
| VV : $CO_2(g) + 8H^+ + 8e^- = CH_4(g) + 2H_2O(l)$ | 0.16 | -0.54 | 0.70 |
| VV : $2CO_2(l) + 12H^+ + 12e^- = CH_3CH_2OH(l) + 3H_2O(l)$ | 0.08 | -0.53 | 0.61 |

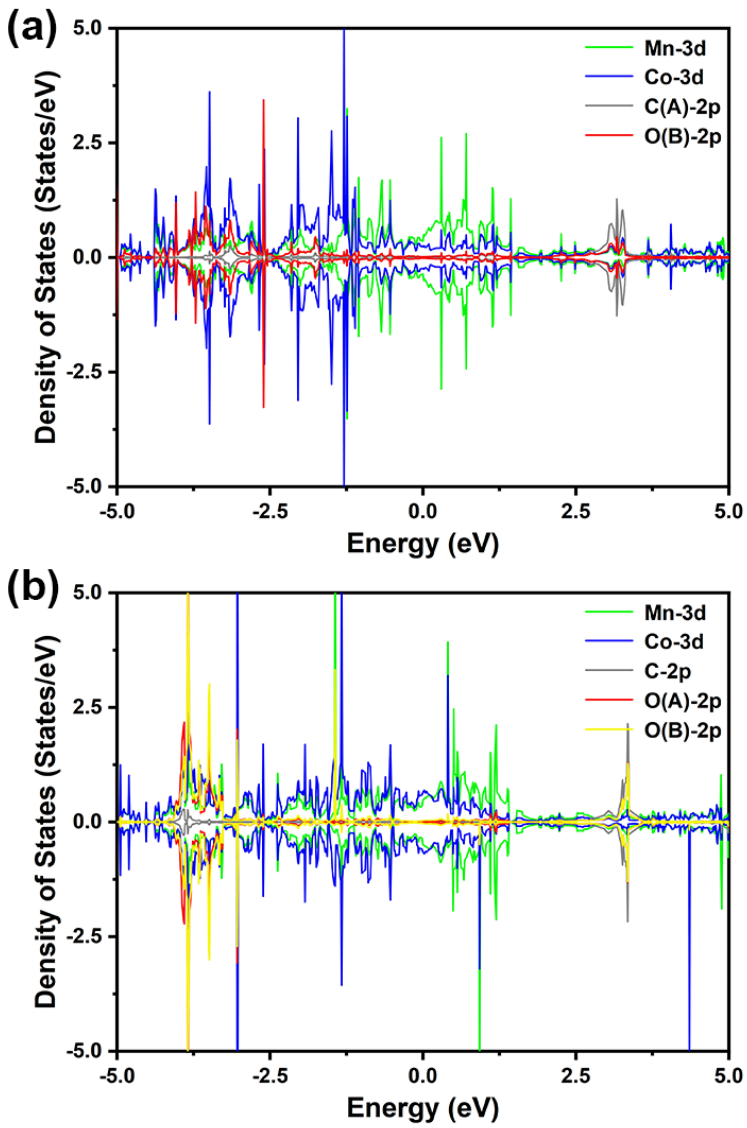


**Figure S8.** The projected density of states of (a) *COOH and (b) *HCOO for MnCo@$\beta_{12}$-B system.

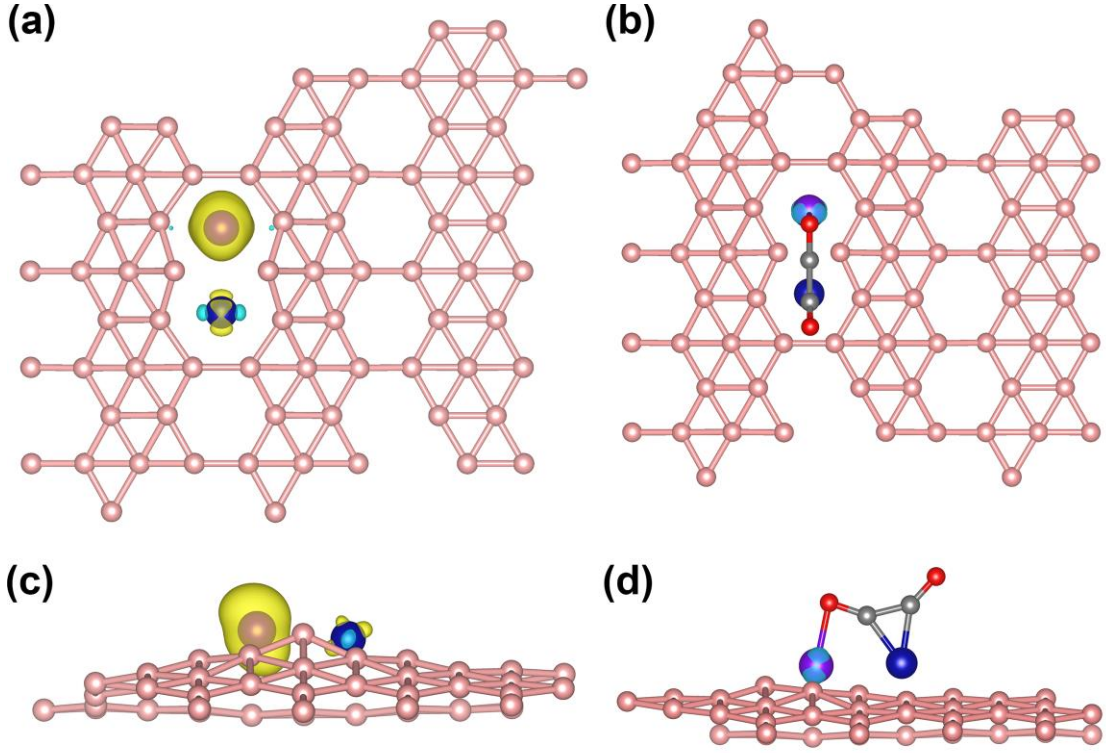


**Figure S9**. The top view and the side view of net spin density of MnCo@$\beta_{12}$-B system and *COCO for MnCo@$\beta_{12}$-B system at an isosurface value of $5 \times 10^{-3}$ e Å$^{-3}$.

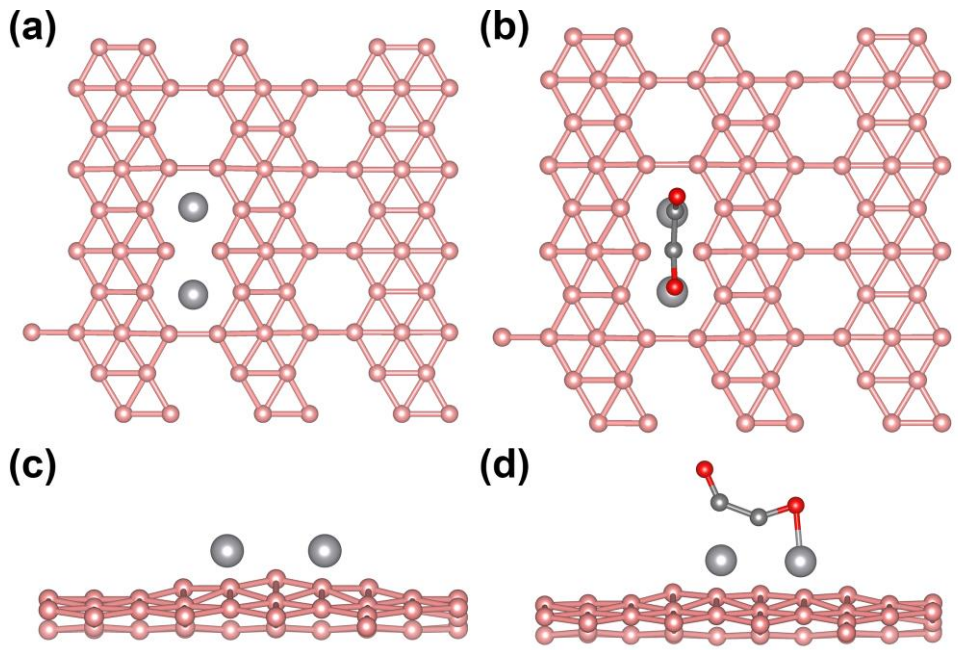


**Figure S10.** The top view and the side view of net spin density of VV@$\beta_{12}$-B system and *COCO for VV@$\beta_{12}$-B system at an isosurface value of $5 \times 10^{-3}$ e Å$^{-3}$.

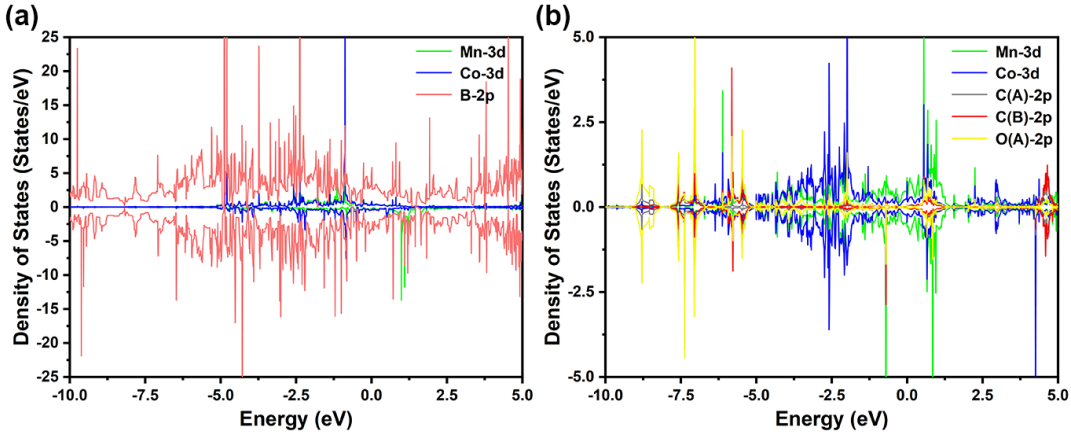


**Figure S11.** The projected density of states of MnCo@$\beta_{12}$-B system and *COCO for MnCo@$\beta_{12}$-B system.

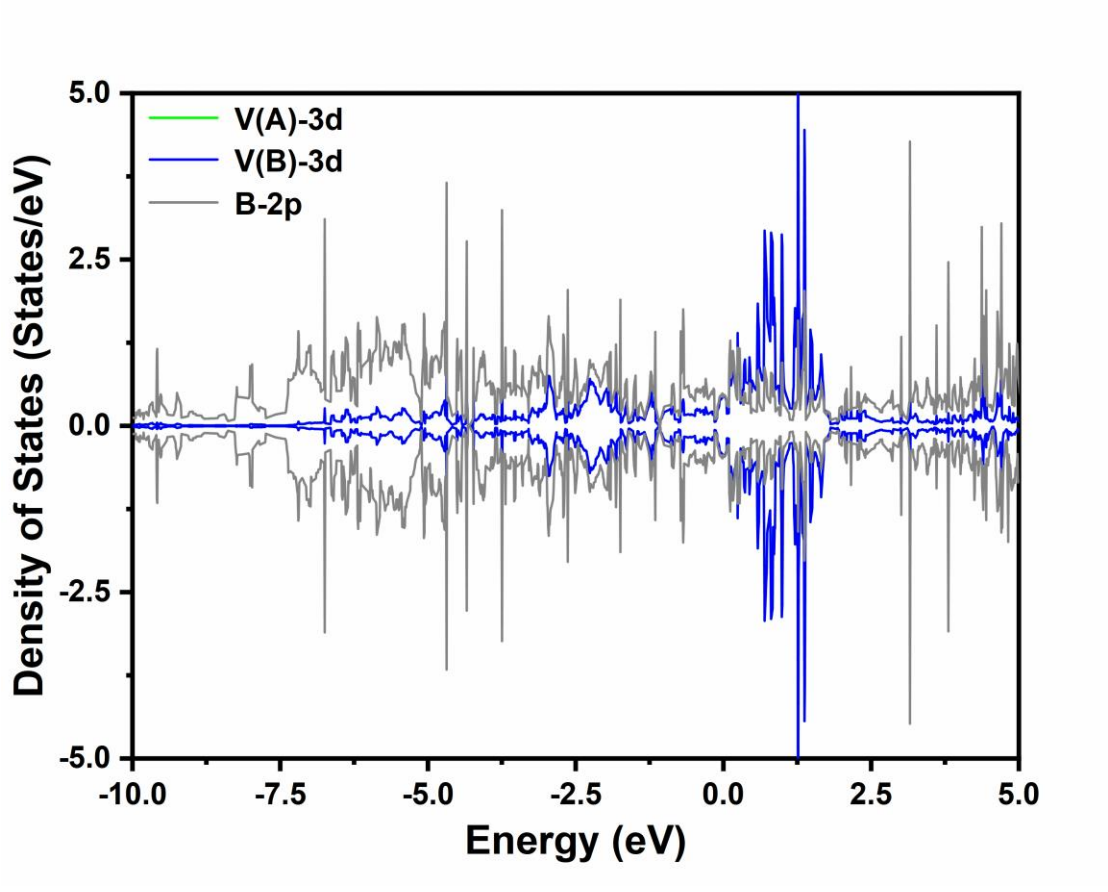


**Figure S12.** The projected density of states of VV@$\beta_{12}$-B system and *COCO for VV@$\beta_{12}$-B system.

1. A. J. Bard, R. Parsons and J. Jordan, Standard potentials in aqueous solutions, *CRC press*, **1985.**